Atmos. Chem. Phys., 18, 16829–16844, 2018
https://doi.org/10.5194/acp-18-16829-2018

Atmospheric Chemistry and Physics
Open Access
EGU

The influence of photochemical aging on light absorption of atmospheric black carbon and aerosol single-scattering albedo

Xuezhe Xu[1,2], Weixiong Zhao[1], Xiaodong Qian[1,2], Shuo Wang[1,2], Bo Fang[1], Qilei Zhang[1,2], Weijun Zhang[1,2,3], Dean S. Venables[4], Weidong Chen[5], Yong Huang[6,7], Xueliang Deng[6,7], Biwen Wu[6,7], Xinfeng Lin[7,8], Sen Zhao[7,8], and Yingxiang Tong[7,8]

[1]Laboratory of Atmospheric Physico-Chemistry, Anhui Institute of Optics and Fine Mechanics, Chinese Academy of Sciences, Hefei, 230031, Anhui, China
[2]Graduate School, University of Science and Technology of China, Hefei, 230026, Anhui, China
[3]School of Environmental Science and Optoelectronic Technology, University of Science and Technology of China, Hefei, 230026, Anhui, China
[4]School of Chemistry and Environmental Research Institute, University College Cork, Cork, Ireland
[5]Laboratoire de Physicochimie de l'Atmosphère, Université du Littoral Côte d'Opale, 59140 Dunkerque, France
[6]Anhui Institute of Meteorological Science, Hefei, 230031, Anhui, China
[7]Shouxian National Climatology Observatory, Shouxian, 232200, Anhui, China
[8]Anhui Shouxian Meteorological Bureau, Shouxian, 232200, Anhui, China

Correspondence: Weixiong Zhao (wxzhao@aiofm.ac.cn) and Weijun Zhang (wjzhang@aiofm.ac.cn)

Received: 21 January 2018 – Discussion started: 26 March 2018
Revised: 13 November 2018 – Accepted: 19 November 2018 – Published: 29 November 2018

Abstract. Coating enhancement of black carbon (BC) light absorption (E_{abs}) is a large uncertainty in modelling direct radiative forcing (DRF) by BC. Reported E_{abs} values after atmospheric aging vary widely and the mechanisms responsible for enhancing BC absorption remain elusive. Here, we report on the direct field measurement of size-resolved mixing state, E_{abs}, and aerosol single-scattering albedo (SSA) at $\lambda = 532$ nm at a rural site in east China from June to July 2016. Strong diurnal variability of E_{abs}, SSA, and O_x ($O_x = NO_2 + O_3$, a proxy for atmospheric photochemical aging) was observed. A method that combined E_{abs} and SSA was developed to retrieve the fraction contribution of BC absorption (f_{BC}), lensing-driven enhancement (f_{Lens}), as well as the fractional contribution of coating absorption (fraction absorption contribution (f_{Shell}), the coated shell diameter (D_{Shell}) and the imaginary part of the complex refractive index (CRI) of the shell (k_{Shell})). Parameterization of E_{abs} and SSA captures much of the influence of BC coating and the particle absorption. In our measurements at this site, the results showed that the absorption amplification depended on the coating thickness and the absorption of coating materials, and photochemistry plays a role in modifying the absorption of BC-containing particles. The lensing-driven enhancement was reduced by light absorption of the shell. One implication of these findings is that the contribution of light-absorbing organic compounds (brown carbon, BrC) at a longer aging time should be included in climate models.

1 Introduction

Black carbon (BC) is the most efficient light-absorbing component of atmospheric aerosols (Jacobson, 2001; Moffet and Prather, 2009; Cappa et al., 2012) and plays an important role in the global climate system (Ramanathan and Carmichael, 2008; Bond et al., 2013). However, accurately constraining the direct radiative forcing (DRF) of BC is a challenge owing to the discrepancy between observed and modelled estimates of BC light absorption (Gustafsson and Ramanathan, 2016). For example, a recent study has shown that the improved model-estimated DRF of BC ($+0.21\ Wm^{-1}$) by including BC absorption enhancement and separately treating the aging and physical properties of fossil fuel and biomass burning BC was about 3 times lower than the values reported in the

Intergovernmental Panel on Climate Change (IPCC) 5th assessment report ($+0.6\,\mathrm{Wm^{-2}}$), which suggested an overestimation of BC lifetime and an incorrect absorption attribution of light-absorbing organic compounds (brown carbon, BrC) (X. Wang et al., 2014).

BC particles are produced from incomplete combustion of fossil fuels, biofuels, and residual biomass (Novakov et al., 2003; Bond et al., 2004, 2007). Freshly emitted BC is mainly externally mixed and occurs in fractal-like agglomerates. Atmospheric BC particles undergo several aging processes, including coagulation with other particles, condensation of vapours onto surfaces, and chemical oxidation (Slowik et al., 2004; Zhang et al., 2008; Petzold et al., 2013). Individual BC particles become coated (i.e., internally mixed) with sulfate, ammonium, organics, nitrate, and water (Bond and Bergstrom, 2006; Cheng et al., 2006; Schwarz et al., 2008; Ervens et al., 2010; Zaveri et al., 2010). Aging processes dramatically change the morphology, hygroscopicity, and mixing state of BC-containing particles, thereby altering their optical properties and the magnitude of their contribution to climate forcing (Jacobson, 2001; Bond and Bergstrom, 2006; Schwarz et al., 2008; Zhang et al., 2008).

The light absorption enhancement of BC particles caused by coating is quantified by E_{abs}, the ratio of the absorption coefficients of coated and bare BC. E_{abs} introduces a large uncertainty in the DRF of BC, which is the second most important contributor to global warming (Jacobson, 2001; S. Liu et al., 2015). Current models simply adopt a constant enhancement value (~ 1.5 or 2) for the calculation of DRF of BC (Cappa et al., 2012; Bond et al., 2013; X. Wang et al., 2014). In contrast, reported E_{abs} values vary widely (Peng et al., 2016; Liu et al., 2017). Field measurements along the California coast and ground site in Sacramento (California) (Cappa et al., 2012), Shenzhen (South China) (Lan et al., 2013), the Nagoya urban area (Japan) (Nakayama et al., 2014), and urban Los Angeles (USA) (Krasowsky et al., 2016) found negligible absorption enhancement ($E_{\mathrm{abs}} < 1.1$) and weak dependence on the extent of photochemical aging (estimated from the value of $-\log([\mathrm{NO}_x]\,/\,[\mathrm{NO}_y])$, where $\mathrm{NO}_x = \mathrm{NO} + \mathrm{NO}_2$ and NO_y includes the sum of NO_x and its oxidation products; Deolal et al., 2012). Biomass burning measurements showed an absorption enhancement of 1.7 at $\lambda = 532\,\mathrm{nm}$ (Lack et al., 2012). Recent observations in Chinese cities (Peng et al., 2016; X. Cui et al., 2016; Xu et al., 2016; Chen et al., 2017; Cheng et al., 2017; Q. Wang et al., 2017) provide evidence for a higher E_{abs} in polluted conditions, with values ranging from 2 to 3. The mechanisms responsible for enhancing BC absorption remain elusive due to the complexity of the aging process and its varied sources. More studies in receptor locations with a longer BC aging time are required to better constrain E_{abs} (Gustafsson and Ramanathan, 2016; Boucher et al., 2016).

In this work, the influence of photochemical aging on BC mixing state, E_{abs}, and aerosol single-scattering albedo (SSA, ω, defined as the ratio of scattering to extinction coefficient) at a rural site in east China during the summer was studied by using a volatility tandem differential mobility analyser (VTDMA) and a thermal denuder (TD) approach combined with a cavity-enhanced albedometer operating at $\lambda = 532\,\mathrm{nm}$. In summer, O_x ($\mathrm{O}_x = \mathrm{O}_3 + \mathrm{NO}_2$) exhibits good correlation with secondary pollutants (Zhou et al., 2014; Cevik et al., 2016; Ji et al., 2016). The concentration of O_x was used as a proxy for atmospheric photochemical aging (Hallquist et al., 2016; Q. Wang et al., 2017). We find that photochemical aging results in the growth of particle coating and higher fractions of internally mixed BC particles. The modelling and parameterization of E_{abs} and SSA capture the variability of BC coating amount and the particle absorption and provide a plausible new method to better constrain the contribution of BC to the DRF.

2 Experimental

2.1 The field site

Measurements were performed at Shouxian National Climatological Observatory (32°25′47.8″ N, 116°47′38.4″ E) in Anhui Province from 16 June to 23 July 2016. Shouxian County is located in China's north–south climate transition zone and is affected by the east Asian monsoon. The new observatory is situated about 15 km south of the previous, historically important observation site (Fan et al., 2010; Li et al., 2011; Deng et al., 2012); it is a rural background site surrounded by basic farmland protection areas and has no significant industrial pollution sources or tall buildings nearby.

Instruments were installed in a temperature-controlled room with two sample inlets about 1 m above the roof (Fig. S1 in the Supplement). Each inlet consisted of one $\mathrm{PM}_{2.5}$ cyclone (BGISCC2.654) with a 50 % cut point at 2.5 µm, and was first dried below 40 % relative humidity (RH) using a diffusion drier. The sampling rates at both inlets were controlled with mass flow controllers (MFCs) and set at $10\,\mathrm{L\,min^{-1}}$. One of the inlets was used for the volatility measurements; the other inlet stream was used for the optical measurements. Trace gas pollutants such as CO, NO_x, SO_2, and O_3 were, respectively, measured by Thermo 48i, 42i, 43i, and 49i analyser.

2.2 Volatility measurement

Size-resolved mixing state of BC was measured with a VTDMA developed in-house. The VTDMA was structurally similar to other systems described in the literature (Cheng et al., 2009, 2012; Wehner et al., 2009; Cheung et al., 2016) and comprised the following:

1. an electrostatic classifier (DMA, differential mobility analyser, TSI 3080) for the initial selection of monodisperse particles;

2. a custom-built stainless steel heating tube (inner diameter of 0.77 cm, 80 cm long, and heated to 300 ± 5 °C) for removing nonrefractory particulate matter; and

3. a scanning mobility particle sizer (SMPS, TSI 3936) comprising a DMA (TSI 3080) and a condensation particle counter (CPC, TSI 3776) for measuring the size distribution of the heated sample in the range of 15 to 661 nm.

Diffusion losses and the effect of multicharged particles were corrected by the instrument software. The residence time of the sample in the heating tube was about 1.2 s and is comparable with other VTDMA systems (0.3–1 s) (Brooks et al., 2002; Philippin et al., 2004; Villani et al., 2007).

2.3 Optical measurement

The optical properties of dry $PM_{2.5}$ particles were measured with a cavity-enhanced albedometer operating at $\lambda = 532$ nm (Zhao et al., 2014; Xu et al., 2016). The albedometer combined broadband cavity-enhanced spectroscopy (BBCES) with an integrating sphere (IS) for direct, in situ, and simultaneous measurement of extinction (b_{ext}) and scattering (b_{scat}) coefficients, thus allowing the calculation of the absorption (b_{abs}) coefficient and SSA. Compared with our previously reported 470 nm system (Zhao et al., 2014; Xu et al., 2016), the new 532 nm albedometer was modified by inserting a quartz tube within the IS to prevent the degradation of the IS reflectivity and to reduce the sample's residence time (Dial et al., 2010; Onasch et al., 2015). The sample volume of the albedometer was about 0.3 L and the flow rate was 1.5 L min^{-1} at atmospheric pressure.

The details of the evaluation of the instrument have been described in our previously published paper (Zhao et al., 2014; Xu et al., 2016; Fang et al., 2017). Detection limits of each parameter were determined by using an Allan variance analysis. With a 30 s integration time (an average of 300 individual spectra, each with 100 ms exposure time), the detection limits under ambient aerosol loading condition for the scattering and extinction measurements were better than 0.15 and 0.12 Mm^{-1}, respectively. The accuracy of the instrument was evaluated with laboratory-generated, NIST traceable monodispersed polystyrene latex (PSL) spheres. During field observations, the optical system was calibrated with N_2, CO_2, and PSL every 2 weeks.

The total uncertainties (summed in quadrature of each error source) in extinction, scattering, absorption coefficients, and SSA measurements were estimated to be less than 4 %, 3 %, 5 %, and 4 %, respectively. Uncertainty in extinction mainly arose from the uncertainties in mirror reflectivity (1 – R, ∼ 1 %), the ratio of cavity length to the cell length containing the air sample when the cavity mirrors were purged (R_L, ∼ 3 %), and particle losses in the cavity (∼ 2 %). Uncertainty in the scattering measurement was mainly caused by uncertainties in the experimentally determined scattering calibration coefficient (K', ∼ 2 %), particle losses in the cavity (∼ 2 %), and the truncated fraction of total scattering. (Since most particles in the observation were smaller than 1 µm, the uncertainty associated with truncation angle was < 1 %, as discussed in Sect. S2 in the Supplement.) Since measurements of the extinction and scattering coefficients were of the identical sample, particle losses do not affect the SSA measurement (Zhao et al., 2014; Xu et al., 2016).

The sampled ambient air was divided into two channels: the first channel was directly pumped into the albedometer to measure the ambient absorption coefficient ($b_{abs,ambient}$); another channel was installed with a TD (Dekati Ltd., Finland) operating at 300 °C to evaporate semi-volatile particulate components for measuring the absorption coefficient of refractory BC (rBC; $b_{abs,TD}$) (Olson et al., 2015). These two channels were switched automatically every 5 min with an electric ball valve. The flow rate of the TD was 10 L min^{-1}. Particle losses inside the TD are discussed in detail in Sect. S3 in the Supplement and are generally caused by diffusional and thermophoretic processes (Wehner et al., 2002; Fierz et al., 2007). The optical loss of the TD of ambient aerosol was estimated to be ∼ 32 %. The measured $b_{abs,TD}$ was corrected with the particle losses for further calculation of the absorption enhancement ($E_{abs} = b_{abs,ambient} / b_{abs,TD}$). The total uncertainty in E_{abs} measurement was about 9 % (mainly contributed by uncertainties in the measurement of $b_{abs,ambient}$ (5 %), $b_{abs,TD}$ (5 %), and particle losses inside TD (6 %)).

3 Results and discussion

The concentrations of $PM_{1.0}$, $PM_{2.5}$, and trace pollutants (CO, NO_2 and O_3) measured at the station over the measurement period are shown in Fig. 1. For assessing the effect of photochemical oxidation on the aerosol optical properties, the time series of the O_x concentration is also shown in the figure. Both O_x, PM_1 and $PM_{2.5}$ concentrations have clear diurnal cycles. The corresponding meteorological conditions are shown in the Supplement Fig. S8. The average ambient temperature (T), relative humidity (RH), and wind direction (WD) were 26.0 ± 3.3 °C, 90 ± 11 %, and 2.0 ± 1.1 m s^{-1}, respectively. The prevailing winds were southerly. Generally, the low wind speed favoured the accumulation of pollutants, and the RH was also quite high. The average concentrations of $PM_{2.5}$ and $PM_{1.0}$ were 28 ± 14 and 25 ± 13 µg m^{-3}, respectively. The 48 h backward trajectories ending at 500 m above ground level at the Shouxian site are shown in Fig. S9 in the Supplement. The trajectories were aggregated into five groups after taking into account the wind direction, speed, and the geometric distance between individual trajectories (S. Wang et al., 2017). The air masses in clusters 1, 3, 4, and 5 originated from long-range transport with high speeds for over 40 h. Air masses in cluster 2 originated from the vicinity of Anhui province and moved slowly. The long aging time

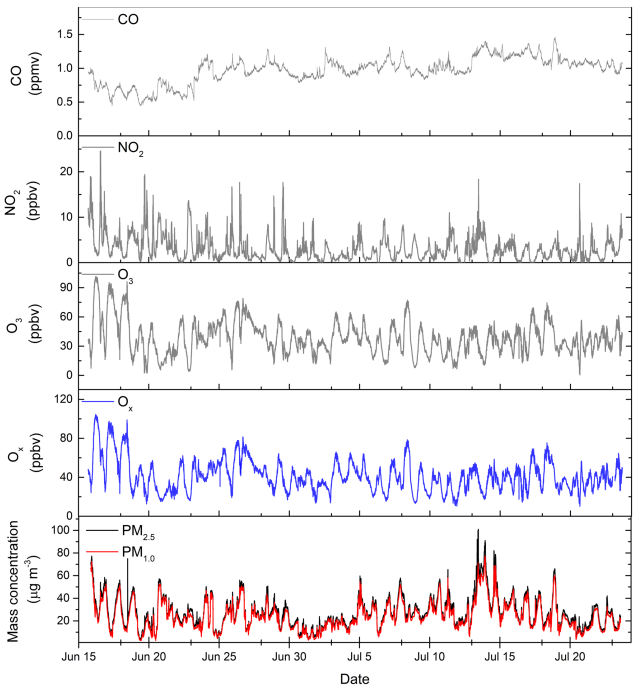

Figure 1. Time series of CO, NO_2, O_3, and O_x ($O_3 + NO_2$) concentrations, as well as the concentrations of $PM_{2.5}$ and $PM_{1.0}$ during the measurement period.

and residence time of the air masses led to well-aged particles before arriving at the observation site. All air masses were at relatively low altitudes (< 1500 m) and remained within the boundary layer over this 2-day period.

3.1 Size-resolved mixing state of BC

Following the approach of Philippin et al. (2004), Cheng et al. (2009), and Wehner et al. (2009), most compounds were assumed to be volatilized at 300 °C and the residual non-volatile particles were regarded as rBC. An example of the measured size distribution is shown in Fig. 2. The heated size distribution was divided into three size ranges – "high-volatility" (HV), "medium-volatility" (MV), and "low-volatility" (LV) – to calculate the number fraction of internally mixed BC particles:

$$F_{\text{in}} = N_{\text{MV}} / (N_{\text{MV}} + N_{\text{LV}}), \quad (1)$$

where N_{MV} is the number concentration of MV particles and is considered to be internally mixed BC. N_{LV} is the number concentration of LV and is considered to be externally mixed BC (Cheng et al., 2009, 2012; Wehner et al., 2009; Cheung et al., 2016).

To assess the influence of atmospheric photochemical aging on the mixing state of BC, scatter plots of F_{in} at different diameters and O_x concentrations are shown in Fig. 3. Data points are colour-coded with respect to the concentrations of CO, which is related to primary BC emission. The value of F_{in} reflects the competition between fresh emission and atmospheric aging (Cheng et al., 2012). The freshly emitted particles have lower F_{in} values, while the aging process converts externally mixed particles into internally mixed and then increases the value of F_{in}. In this work, low F_{in} values tended to appear at high CO concentrations, consistent with freshly emitted BC. The observed decreasing trends in F_{in} with O_x for particle diameters of 50 and 100 nm were probably due to the increment of the relative contribution of fresh emissions in the small particle size range.

A positive correlation between F_{in} and O_x was observed for particle diameters of 150, 200, 250, and 300 nm, respectively. The corresponding oxidation rates of F_{in} were 0.07 and 0.12 % ppb^{-1} and 0.16 %, and 0.17 % ppb^{-1}. Particles of these sizes have greater internal mixing and may be more susceptible to photochemical oxidation processes. Very recently, Q. Wang et al. (2017) reported a similar correlation between the number fraction of thickly coated rBC (F_{rBC}, the mixing state of individual rBC was measured with single particle soot photometer, SP2) and O_x concentration in highly polluted megacities. The reported oxidation rates of F_{rBC} were 0.58 % ppb^{-1} for Beijing and 0.84 % ppb^{-1} for Xi'an, respectively. Photochemical aging resulted in higher amounts of internally mixed BC and a larger fraction of thickly coated BC under more oxidizing conditions.

3.2 Temporal and diurnal variations in optical properties

Time series of the measured optical properties are shown in Fig. 4 and include the extinction (b_{ext}), scattering (b_{scat}), and absorption (b_{abs}) coefficients, the SSA for ambient particles (b_{ambient}) and for particles passed through TD (b_{TD}), and the corresponding E_{abs}. The mean (and standard deviation) of $b_{\text{ext,ambient}}$, $b_{\text{scat,ambient}}$, and $b_{\text{ext,TD}}$, $b_{\text{scat,TD}}$ were 92 ± 64, 81 ± 55, 12 ± 7, and 6.5 ± 4.1 Mm^{-1}, respectively. The scattering fraction remaining ($b_{\text{scat,TD}} / b_{\text{scat,ambient}}$) was about 0.09 ± 0.05 and indicated that most of the coating species evaporated in the TD at 300 °C. Our value is comparable to the value of 0.08 ± 0.02 reported by Nakayama et al. (2014). The change in the morphology during heating was negligible.

The observed diurnal variation in optical parameters ($b_{\text{ext,ambient}}$, $b_{\text{scat,ambient}}$, ω_{ambient}, $b_{\text{abs,ambient}}$,$b_{\text{ext,TD}}$,$b_{\text{scat,TD}}$, $b_{\text{abs,TD}}$, ω_{TD}, E_{abs}), mass concentrations of $PM_{2.5}$, as well as the mixing ratio of CO and the photochemical oxidant (O_x) are shown in Fig. 5. Broadly similar diurnal patterns were observed for the extensive optical properties ($b_{\text{ext,ambient}}$, $b_{\text{scat,ambient}}$, $b_{\text{abs,ambient}}$, $b_{\text{ext,TD}}$, $b_{\text{scat,TD}}$, $b_{\text{abs,TD}}$) of ambient particles and particles passed through the thermodenuder, and the mass concentrations of $PM_{2.5}$. A strong diurnal variation and similar diurnal patterns in ω_{ambient}, ω_{TD}, E_{abs}, and O_x were observed. Patterns of the extensive optical properties and $PM_{2.5}$ indicate some local particle emissions from early morning anthropogenic activities. While these changes

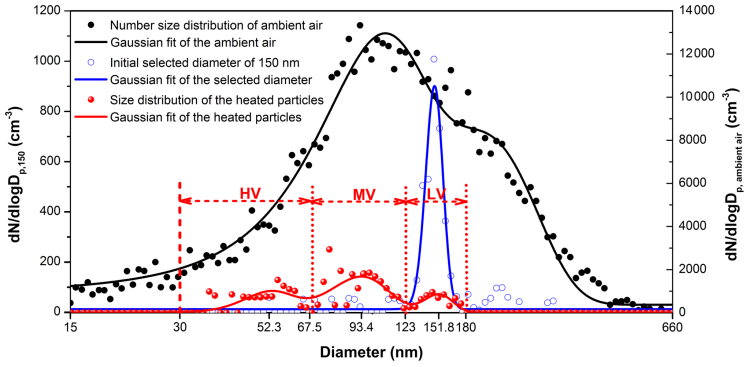

Figure 2. Examples of the particle number size distributions of ambient aerosol (black points), as well as the VTDMA measured room temperature bypass sample (~ 25 °C, blue open circles), and the sample passed through a custom-built heating tube at 300 °C ($D_{p,300\,°C}$, red points) for the initial selected diameter of 150 nm (D_p). The corresponding Gaussian fit of the size distributions are shown as black, blue, and red lines. The size distribution obtained after heating was divided into three size ranges according to previously reported empirical cutting diameters. (1) Particles with diameters $D_{p,300\,°C} / D_p < 45\,\%$ were denoted as "high-volatility" (HV) and were not considered to be BC. (2) Particles with diameters $45\,\% < D_{p,300\,°C} / D_p < 82\,\%$ were considered to be internally mixed BC particles (a non-volatile core coated with a volatile shell) and were denoted as "medium-volatility" (MV). (3) Particles with diameters $82\,\% < D_{p,300\,°C} / D_p < 120\,\%$ were denoted as "low-volatility" (LV) and were considered to be externally mixed BC.

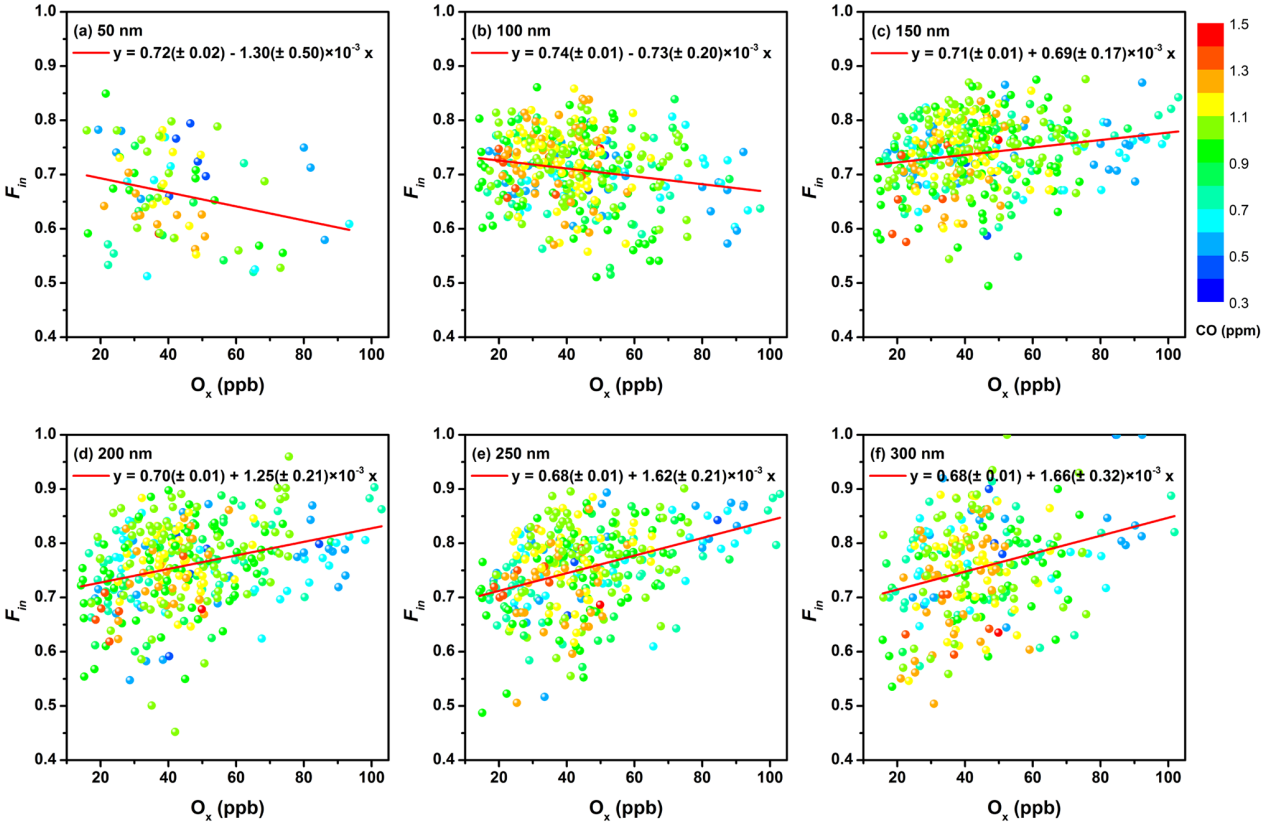

Figure 3. Correlation between the hourly-averaged number fractions of internally mixed BC (F_{in}) and the photochemical oxidant (O_x) mixing ratios for different size bins (50, 100, 150, 200, 250, and 300 nm). Data points are colour-coded with respect to the concentrations of CO (an indicator of primary BC emissions). Low F_{in} values generally appear at high CO concentrations, and vice versa. For 150, 200, 250 and 300 nm diameters, F_{in} values increased with oxidant concentration. The slope of the linear regression (red line) is representative of the oxidation rate of F_{in} (the fit standard error is shown in brackets).

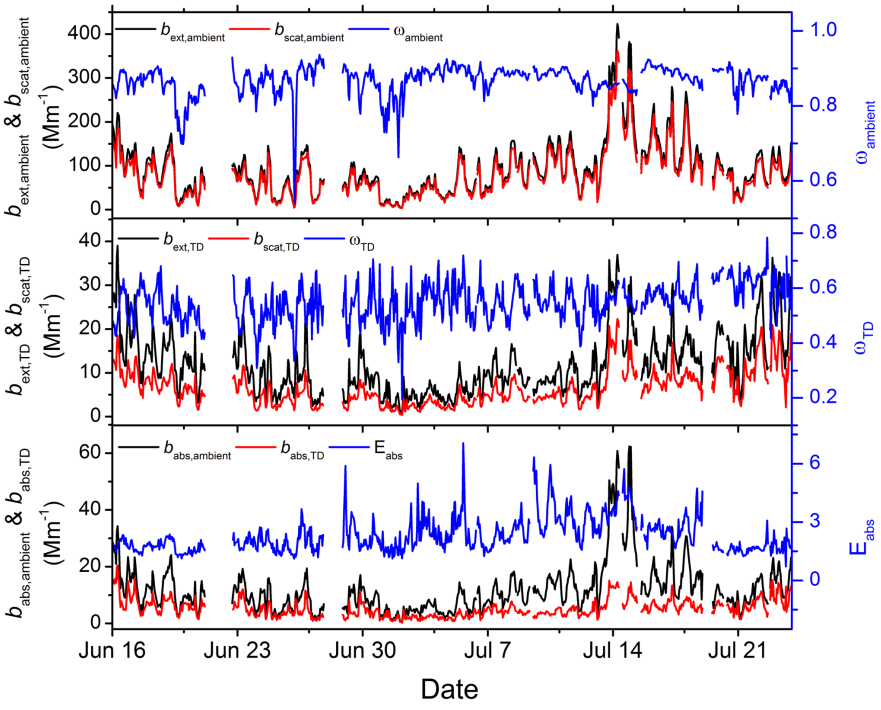

Figure 4. Time series of the optical parameters and absorption enhancement (E_{abs}) at $\lambda = 532$ nm at a time resolution of 10 min. Properties shown are the extinction (b_{ext}), scattering (b_{scat}), and absorption coefficients (b_{abs}), the SSA (ω) of ambient particles ($b_{ambient}$), and particles passed though the thermodenuder (b_{TD}) at 300 °C (after correcting for particle losses).

are radiatively significant, changes in $PM_{2.5}$ during the early daylight period are weak, suggesting that emitted particles are small and contribute little to the overall particle mass concentration. The SSA shows that particles tend to be more strongly absorbing in early morning than later in the day; however, measured SSA values are not especially low (mean $\omega_{ambient} \geq 0.85$), consistent with the background nature of the Shouxian site. Thus, freshly emitted particles are therefore relatively unimportant at this site. CO concentrations show minor diurnal variation, consistent with the regional nature of air masses at this site.

Daytime increases in the boundary layer into the mid-afternoon are especially evident in the $PM_{2.5}$ concentration profile. In contrast, ambient scattering and extinction profiles are broadly flat over the same period, indicating more intense photochemical processing and extensive secondary aerosol generation. The same effect is responsible for the mid-afternoon maximum in the intensive optical property $\omega_{ambient}$.

3.3 Influence of photochemical aging on E_{abs} and SSA

SSA is one of the most relevant intensive optical properties (Jo et al., 2017) because it describes the relative strength of the aerosol scattering and absorption capacity and is a key input parameter in climate models. Changes in particle size, morphology, chemical composition, and mixing state caused by atmospheric chemical aging processes will alter SSA. The relationships between hourly-averaged ω, ω_{TD}, and E_{abs} with hourly-averaged O_x, as well as the scattering plot of hourly averaged ω, ω_{TD}, and E_{abs} that binned in O_x (with the same data points in each bin) and the frequency distributions of the hourly averaged data are shown in Fig. 6. Approximately 90 % of the values of ω, ω_{TD}, and E_{abs} during the measurement were within the range of 0.80–0.91, 0.43–0.65, and 1.0–3.5, respectively.

During the summer, O_3 has a central role in the generation of secondary aerosol. Positive correlations between ω, ω_{TD}, and O_x concentrations were observed in our measurements (Fig. 6a and b), which suggests that higher O_x actually increases the mass fraction of secondary aerosol particles and the overall ensemble of particle material and SSA. Our result is consistent with Beijing summer observations, where SSA was linearly correlated with the mass fractions of secondary aerosols (Han et al., 2017). The increase in ω_{TD} resulted from incomplete vaporization of non-volatile constituents in the heating tube (Cheung et al., 2016), the generation of low-volatility oxygenated organic aerosol during photochemical aging (Paciga et al., 2016), and the changes in BC morphology (Radney et al., 2014). Summertime volatility measurement of organic aerosol in the megacity Paris shown that about 10 % mass fraction remained with a TD operating at 180 °C (Paciga et al., 2016). However, recent re-

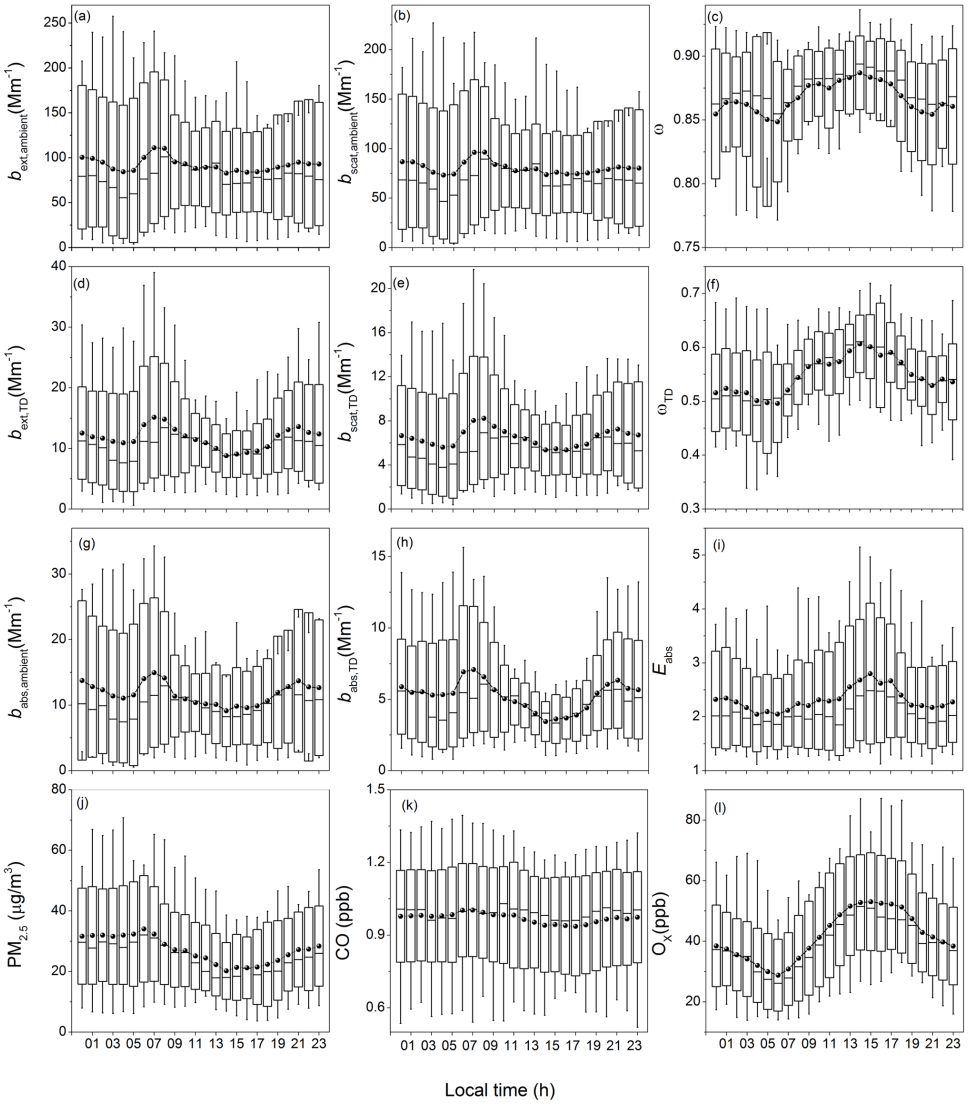

Figure 5. The observed diurnal variation in aerosol optical parameters (extinction (b_{ext}), scattering (b_{scatt}), absorption (b_{abs}) coefficients, and SSA (ω)) of ambient particles ($b_{ambient}$, **a–c**, **g**) and particles passed through the thermodenuder at 300 °C after correcting for particle losses (b_{TD}, **d–f**, **h**). The absorption enhancement (E_{abs}, **i**) was calculated as the ratio between $b_{abs,ambient}$ / $b_{abs,TD}$. The mass concentrations of $PM_{2.5}$ **(j)** and the mixing ratios of CO **(k)** and O_x **(l)** are also shown for assessing the effect of photochemical oxidation. The optical measurement at $\lambda = 532$ nm covered the period 16 June to 23 July 2016. The box and whisker plots show the mean (dots), median (centre solid line), lower and upper quartile (boxes), and 5th and 95th percentile (whiskers).

search demonstrated that the remaining non- and low-volatile coating has a minor impact on the absorption measurement of heated particles using TD operating at 250 °C (S. Liu et al., 2015). Theoretical and experiment results show that aging causes the dramatic changes in BC particle morphology (China et al., 2015; He et al., 2015, 2016; Scarnato et al., 2013; Y. Wang et al., 2017) and leads to more compact black carbon with higher scattering cross sections (Peng et al., 2016; Y. Wu et al., 2018), which in turn results in an increase in ω_{TD} (Radney et al., 2014; Forestieri et al., 2018). In this regard, the rise in ω_{TD} with increasing O_x concentration can be used as an indicator of the changes in BC morphology. The values of ω_{TD} remained stable for O_x mixing ratios larger than 45 ppbv, which possibly indicate that the change in the proportion of non-volatile constituents or BC morphology was negligible.

E_{abs} also rose with higher O_x mixing ratios (Fig. 6c and Fig. S10 in the Supplement), but with a different pattern compared to ω and ω_{TD}. From the scattering plot of the hourly averaged E_{abs} that was binned in O_x, a monotonic growth of E_{abs} with increasing O_x can be observed below 45 ppbv O_x (from 2.1 to 2.6). For O_x mixing ratios between 45 and

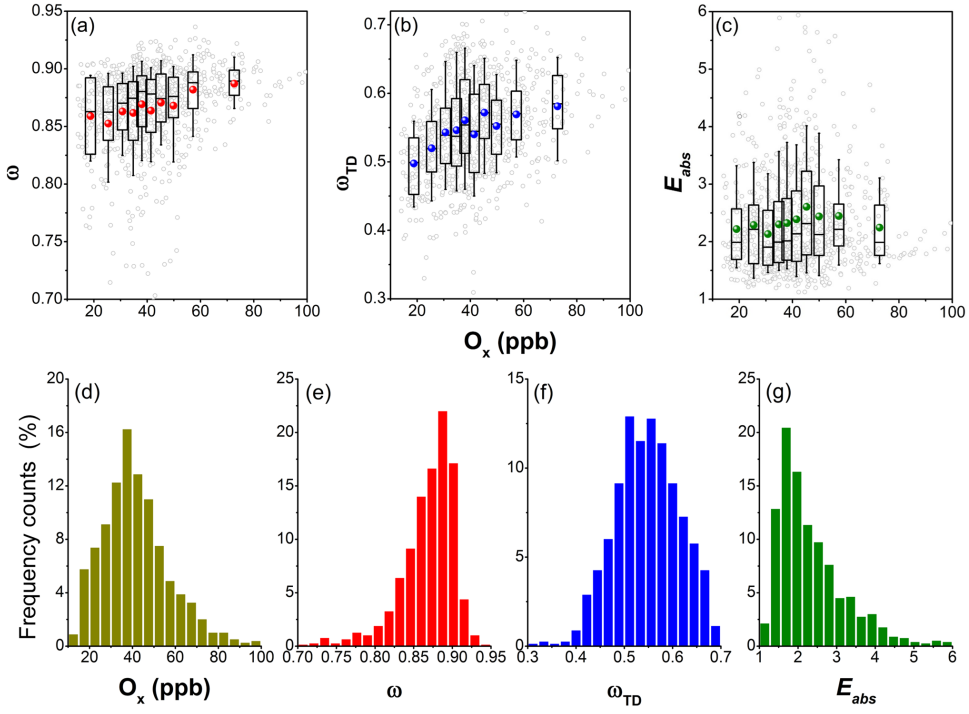

Figure 6. Relationship between **(a)** ω, **(b)** ω_{TD}, and **(c)** E_{abs} with O_x concentrations. The gray circles are the measurement data with 1 h time resolution. The hourly averaged ω, ω_{TD}, and E_{abs} were then binned in O_x with the same data points (80 points) in each bin. The corresponding mean (solid dot), median (centre solid line), lower and upper quartile (boxes), and 10th and 90th percentile (whisker) are shown as the box and whisker plots. The corresponding frequency distribution of each parameters is shown in **(d)**–**(g)**.

57 ppbv, E_{abs} values remained constant ($\sim$2.4). The small drop in E_{abs} value for the O_x bin larger than 57 ppbv was probably caused by the limited data numbers for O_x larger than 75 ppbv and was statistically insignificance. The most frequently occurring value of E_{abs} for the whole measurement was $\sim$1.7.

Since the emission sources, weather conditions, and aging degrees of BC particles varied from day to day, the relationship between E_{abs} and atmospheric chemistry is rather complex. Four selected cases with different wind directions were used to demonstrate this complexity (as shown in Fig. 7, the day- and nighttime data were separated). The corresponding wind directions and speeds, RH values, and CO concentrations are shown in Fig. S10 in the Supplement. The patterns of E_{abs} with O_x were different for air masses from different directions. For cases 1 and 2, the mean values of E_{abs} were comparable (1.9 ± 0.2 for case 1 and 1.8 ± 0.6 for case 2), and the hourly-averaged ω and ω_{TD} grew with increasing O_x in both cases. In case 1, E_{abs} ranged from 1.5 to 2.3, with a growth rate of ~ 0.01 ppbv^{-1} in the daytime. During this period, winds were typically from the north, which corresponding to a short transported pathway of air masses (Fig. S9 in the Supplement). The low degree of aging led to a small E_{abs} value. In case 2, E_{abs} ranged from 1.1 to 3.7, and the corresponding growth rates was ~ 0.05 ppbv^{-1} in the daytime. It is worth noting that the low E_{abs} values in this period corresponded to low ω values (Fig. 7c), which indicated the influence on the local emissions on E_{abs}. For cases 3 and 4, ω and ω_{TD} increased slowly with O_x in comparison with cases 1 and 2. Monotonic relationships were found here, with growth rates of ~ 0.01 and 0.05 ppbv^{-1}. The large E_{abs} values in the daytime than nighttime suggested that photochemistry plays a positive effect on the increment of absorption enhancement. These results demonstrated the complex influence of emission and aging degree of BC particles in modifying the light absorption of BC-containing particles. For air masses from different directions, the relationship between E_{abs} and O_x may be different.

A list of recently reported E_{abs} values is shown in Table 1. The averaged and standard deviation of E_{abs} value at $\lambda = 532$ nm for this work was 2.3 ± 0.9, which agreed well with values from Boulder using the same TD method combined with a photoacoustic spectrometer (PAS) (Lack et al., 2012) from Yuncheng (X. Cui et al., 2016) and Jinan (Chen et al., 2017) using an aerosol filtration–dissolution (AFD) method and from Beijing (Peng et al., 2016; Xu et al., 2016; Cheng et al., 2017) based on the mass absorption efficiency (MAE) method. Our result is also comparable to that reported in laboratory studies of thickly coated BC particles where E_{abs} ranged from 1.8 to 2.4 (Bond et al., 2013).

Table 1. A survey of some field measured E_{abs} values.

Method	Location	E_{abs}	Reference	Description
AFD	Yuncheng, China (rural)	2.25 ± 0.55 (678 nm)	X. Cui et al. (2016)	June–July 2014; ECOC (elemental carbon and organic carbon) analyser. (E_{abs} ranged from 1.4 for fresh combustion emissions to 3 for aged ambient aerosols.)
	Jinan, China (urban)	2.07 ± 0.72 (678 nm)	Chen et al. (2017)	February 2014; ECOC analyser. $E_{abs} \sim 1.3$–1.5 for fresh urban aerosols and $\sim$ 2–2.5 for aged aerosols.
MAE	California, USA (rural)	~ 1.16 (532 nm)	Cappa et al. (2012)	June 2010; absorption coefficients at 405 and 532 nm were measured by PAS; rBC mass concentration was measured with SP2; SP2 measured rBC core diameter $\sim$ 174 nm.
	Shenzhen, China (urban)	1.07 (532 nm)	Lan et al. (2013)	August–September 2011; absorption coefficients at 405, 532, 781 nm measured were measured with PAS; rBC mass concentration was with SP2; $MAE_{532\ nm} = 6.5 \pm 0.5\ m^2\ g^{-1}$ (with lowest value of $6.08\ m^2\ g^{-1}$ and highest value of $8.5\ m^2\ g^{-1}$, respectively, treated as totally, externally mixed, and internally mixed); SP2 measured BC, core diameter $\sim$ 180 nm.
	Xi'an, China (urban)	1.8 (870 nm)	Q. Y. Wang et al., 2014	December 2012–January 2013; light absorption was measured with PAS; rBC concentration was measured with SP2.
	London, UK (rural)	1.8 (405 nm) 1.4 (781 nm)	S. Liu et al. (2015)	February 2012; absorption coefficients at 405 and 781 nm were measured with PAS; rBC mass concentration was measured with SP2; rBC core diameters ranged from 100 to 200 nm.
	Nanjing, China (suburban)	1.6 (532 nm)	F. Cui et al. (2016)	November 2012; absorption coefficients at 405, 532, and 781 nm were measured with PAS; EC mass concentration was determined by ECOC analyser.
	Beijing, China (suburban)	2.6–4.0 (470 nm)	X. Xu et al. (2016)	November 2014–January 2015, for $PM_{1.0}$ particles; absorption coefficient at 470 nm by using a cavity-enhanced EC albedometer; mass concentration was determined by ECOC analyser.
	Beijing, China (urban) chamber study; Houston, USA (urban)	2.4 (405, 532 nm)	Peng et al. (2016)	May–June 2009 in Houston, August–October 2013 in Beijing; absorption coefficients at 405, 532, and 870 nm were measured with PAS.
	Manchester, UK (urban)	1.0–1.3 (532 nm)	D. Liu et al. (2017)	October–November 2014; chamber study and open wood fire measurement; absorption coefficients at 405, 532, and 781 nm were measured with PAS.
	Kanpur, India (urban)	1.8 (781 nm)	Thamban et al. (2017)	January–February 2015; absorption was measured with PAS; rBC concentration was measured with SP2.
	Beijing, China (urban)	3.2–5.3 (365 nm)	Cheng et al. (2017)	Comparison of water-soluble and methanol-soluble organic carbon; theoretical investigation of E_{abs}.
	Beijing and Xi'an, China (urban)	1.9 (532 nm)	Q. Y. Wang et al. (2017)	February 2013, Xi'an, and February 2014, Beijing; absorption was measured with PAS; rBC concentration was measured with SP2.
	Guangzhou, China (Suburban)	1.5 ± 0.5 (550 nm)	C. Wu et al. (2018)	February 2012–January 2013; light absorption was measured with an aethalometer; EC mass concentration was determined by ECOC analyser.
TD	Toronto, Canada (suburban)	1.6–1.9 (550 nm)	Knox et al. (2009)	December 2006 to January 2007; TD operating at 340 °C; optical properties were measured with PAS and aethalometer.
	California, USA (rural)	1.06 (532 nm)	Cappa et al. (2012)	June 2010; TD operating at 250 °C; absorption coefficients at 405 and 532 nm were measured by PAS; SP2 measured rBC core diameter $\sim$ 174 nm.
	Boulder, USA (forest fire)	2.5 (404 nm) 1.4 (532 nm)	Lack et al. (2012)	September 2010; TD operating at 200 °C; absorption coefficients at 404, 532, and 658 nm were measured with PAS; SP2 measured rBC core diameter: 140 ± 10 nm.
	Nagoya, Japan (urban)	781 nm, TD 300 °C 1.10 ± 0.09 (August) 1.02 ± 0.11 (January)	Nakayama et al. (2014)	August 2011, January 2012; TD operating at 100, 300, and 400 °C; absorption coefficients at 405 and 781 nm were measured with PAS.
	London, UK (rural)	1.3 (405 nm) 1.4 (781 nm)	S. Liu et al. (2015)	February 2012; TD operating at 250 °C; absorption coefficients at 405 and 781 nm were measured with PAS; rBC core diameters ranged from 100 to 200 nm.
	Noto Peninsula, Japan (rural)	1.22 (781 nm, ranged coefficients at 405, from 1.07 to 1.38)	Ueda et al. (2016)	April–May 2013; TD operating at 300 or 400 °C; absorption 532, and 781 nm were measured with PAS.
	California, USA (urban)	1.03 ± 0.05 (870 nm)	Krasowsky et al. (2016)	February–March 2015; TD operating at 230 °C; absorption at 870 nm was measured with PAS.
	Shouxian, China (rural)	2.3 ± 0.9 (532 nm)	This work	June–July 2016; TD operating at 300 °C; absorption at 532 nm was measured with a cavity-enhanced albedometer.

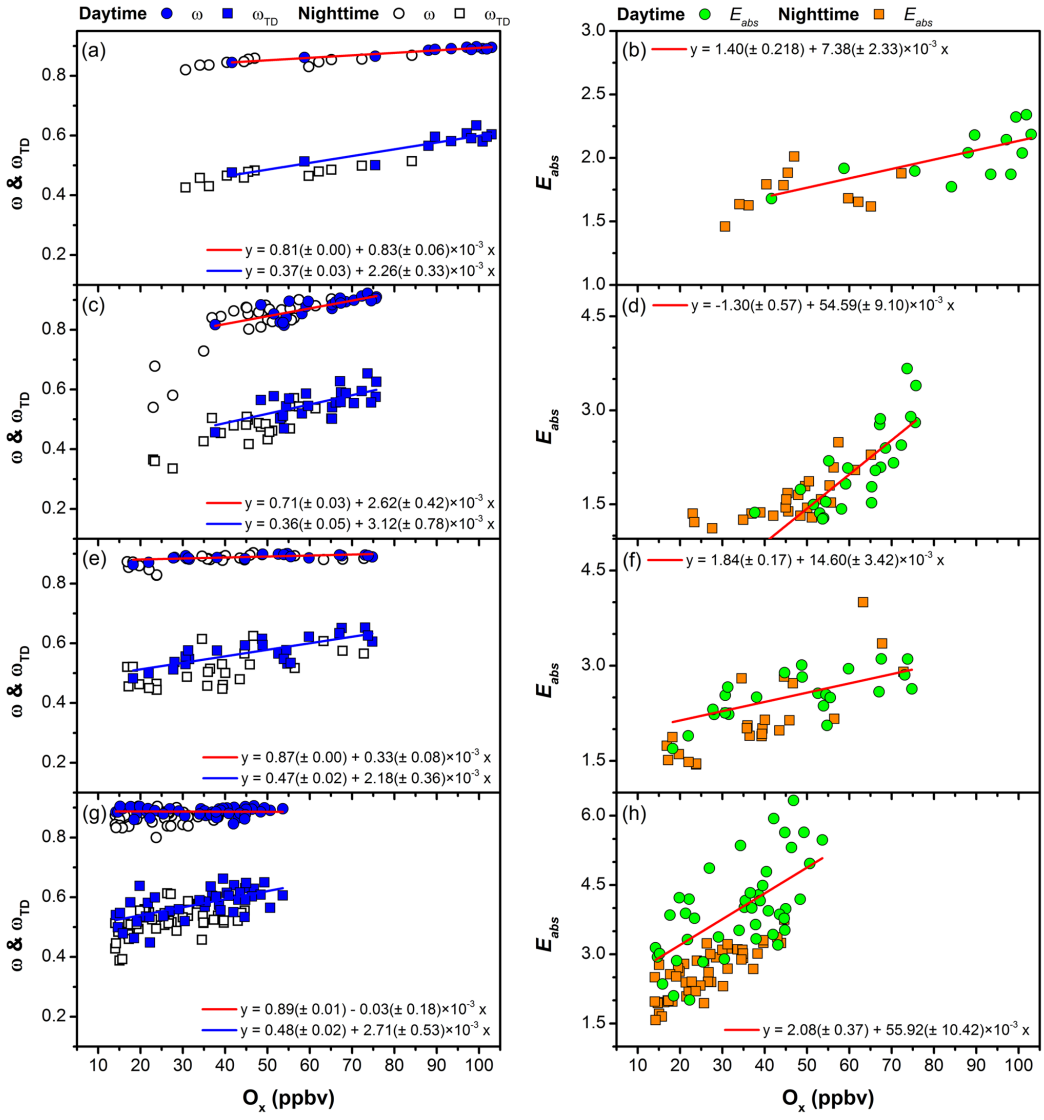

Figure 7. Four selected case studies of the variations in hourly-averaged ω, ω_{TD}, and E_{abs} as a function of hourly-averaged O_x concentrations. **(a, b)** Case 1: on 16 June 2016; winds were typically from the north. **(c, d)** Case 2: 25 to 26 June 2016, wind direction varied from north to south. **(e, f)** Case 3: 7 to 8 July 2016; winds were mainly from the southeast. **(g, h)** Case 4: 9 to 12 July 2016; winds were mainly from the northeast. The daytime (from 06:30 to 18:30 local time) and nighttime (from 18:30 to 06:30 local time) data have been marked in different colours and symbols. The slope of the linear regression (red and blue lines, only for daytime data) is representative of the oxidation rate of each parameter (the fit standard error is shown in brackets).

A chamber study by Peng et al. (2016) suggested that the primary BC was in a chain-like structure with low particle density and then collapsed to a semi-spherical particle. During this stage, there is no significant absorption enhancement (E_{abs} ranged from 1.0 to 1.4). With continued coating growth with several hours' aging in the chamber, the semi-spherical particle was further collapsed and finally transformed to fully compact spherical, internally mixed BC particles (E_{abs} increased to ~2.3–2.4) (Gustafsson and Ramanathan, 2016). Recent morphologically constrained modelling developed by Y. Wu et al. (2018) demonstrated that after full aging, the BC particles became a more compact aggregation, which leads to a stable range of E_{abs} (averaged value ~2.5, with a minimum value of ~2 and a maximum value of ~3.5). Photochemical aging processes lead to internal mixing and a larger coating fraction that enhances the light-absorbing capacity of BC particles (Lack and Cappa, 2010). Our finding of the growth of E_{abs} associated with the increasing O_x concentration suggests that secondary organic aerosol (SOA) includes light-absorbing organic compounds (BrC) (Xu et al., 2016), and that BrC's overall contribution to particle absorption grows under more oxidizing conditions. As discussed in the next

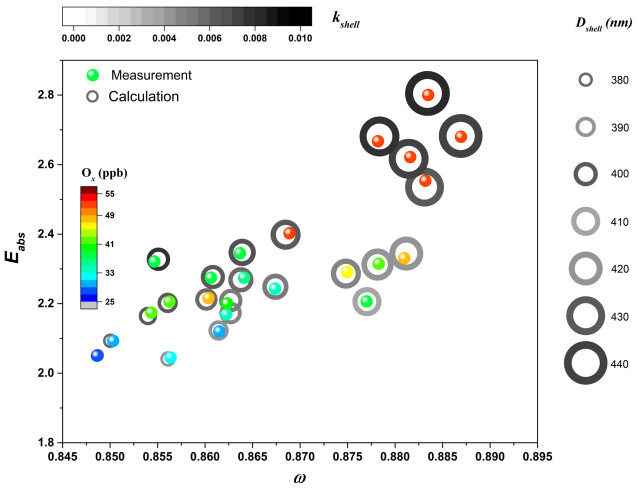

Figure 8. Scatter plot of E_{abs} and ω for different photochemical oxidant concentrations. Variation in the observed diurnally averaged absorption enhancement and SSA (solid points, colour-coded with respect to the concentrations of O_x) is used for the modelling constraint. Both E_{abs} and ω increase with O_x mixing ratio. The open circles are the single-particle Mie theory calculation results with an optimized BC core size of 160 nm. The CRI of BC was fixed at $1.85 + i\ 0.71$. The real part of the CRI of the coating material was fixed at 1.55. The changes in the imaginary part of the CRI and the thickness of the coating material were colour-coded and shown as the different dimensions (open circle).

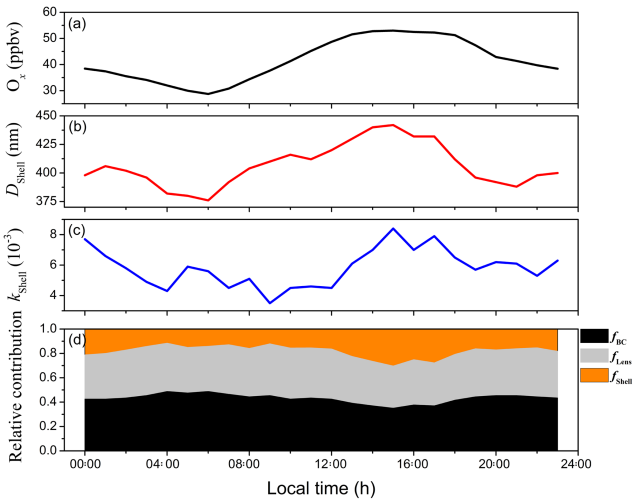

Figure 9. The retrieved diurnal variations in the **(b)** coating thickness (D_{Shell}) and **(c)** imaginary part of the CRI (k_{Shell}) of the coated materials, and **(d)** the relative contribution of the absorption of BC (f_{BC}), lensing effect (f_{Lens}), and absorption of the shell (f_{Shell}). Broadly similar patterns were observed for D_{Shell}, k_{Shell}, f_{Shell}, and **(a)** O_x concentrations.

section, we find an increase in the imaginary part of the complex refractive index (CRI) of the coated shell.

3.4 Coating absorption and light absorption enhancement

Mie theory, which was treated as the basis of the IPCC 5th assessment report due to its computational efficiency and applicability to radiative transfer models (Jo et al., 2017), is a powerful tool for optical data interpretation (Lack et al., 2012) and the reliability of the core–shell model has been verified in many optical closure studies (Lack et al., 2012; Ma et al., 2012; S. Liu et al., 2015; C. Wu et al., 2018). According to Peng et al.'s (2016) chamber study results, BC particles change to a fully compact spherical morphology in less than 1 day. Volatility measurements and analysis of the air masses indicated that the atmospheric aerosol observed in summer at the rural site was well aged. In this work, the particle size distribution information was not available. A method based on single-particle core–shell Mie theory (Bohren and Huffman, 1983; Saleh et al., 2015) was developed to interpret the observed changes in E_{abs} associated with O_x in this work. The sensitivity of this assumption is discussed in Sect. S7 in the Supplement. The modelling was based on simultaneous constraining of E_{abs} and SSA to retrieve the fraction contribution of BC absorption (f_{BC}), lensing-driven enhancement (f_{Lens}), coating absorption (f_{Shell}), as well as the coated shell diameter (D_{Shell}) and the imaginary part of the CRI of the shell (k_{Shell}).

A scatter plot of measured diurnally averaged E_{abs} and SSA for different photochemical oxidant concentrations is shown in Fig. 8. The solid points are the observed results and colour-coded with respect to the concentrations of O_x. The open circles are the single-particle Mie core–shell modelled results with an optimized BC core size of 160 nm and colour- and size-coded with respect to the imaginary part of the CRI of coating material (k_{shell}) and the diameter of coating material (D_{shell}), respectively. The colour-coded plot shows the connection between E_{abs}, SSA, and atmospheric photochemistry. The modelled results are consistent with the observed results. Both SSA and E_{abs} values rise with increasing D_{shell} and k_{shell}, indicating that the coating thickness and absorption play key roles in determining SSA and E_{abs}. Both E_{abs} and SSA increased under more oxidizing conditions. This can be explained by the photochemical production of coating species: with more intense photochemical aging, the fraction of internally mixed BC particles and coating thickness increased. Thickly coated BC was also observed by Q. Wang et al. (2017) under higher O_x mixing ratios.

The corresponding Mie theory calculation results are shown as open circles in Fig. 8 (with further details in Sect. S7 in the Supplement). Comparisons of modelling and observation E_{abs} and SSA are shown as a scatter plot in Supplement Fig. S12. By fixing the BC core diameter, we can retrieve information on the coating shell (D_{Shell}, k_{Shell}) and each contribution to light absorption (f_{BC}, f_{Lens}, f_{Shell}) under different oxidant conditions (Lack and Cappa, 2010), as

shown in Fig. 9. The retrieved D_{shell} ranged from 386 to 440 nm. The corresponding D_{shell} / D_{core} ratio ranged from 2.41 to 2.75, within the range of values (2–4) reported by C. Wu et al. (2018). The plot of measured and modelled E_{abs} with different D_{shell} / D_{core} is shown in the Supplement Fig. S13. The values of k_{shell} ranged from 0.004 to 0.008 with a diurnal average value of 0.006 (±0.001). A comparison of the retrieved k_{shell} with previously reported k values of fresh and aged organic materials is shown in Supplement Fig. S14, which includes BC, BrC aerosol production from biomass burning (BB), atmospheric humic-like substances (HULISs), Suwannee River fulvic acid aerosol (SRFA), and secondary organic material (SOM) produced by photo-oxidation of anthropogenic and biogenic organic precursors. The value of k_{shell} reported here is comparable with those of BB aerosols (Chakrabarty et al., 2010) and SRFA (Bluvshtein et al., 2016), and is larger than those of SOM (Liu et al., 2013; P. Liu et al., 2015), HULIS (P. Liu et al., 2015) and urban BrC (Cappa et al., 2012).

The retrieved diurnal variations in coating shell (D_{Shell}, k_{Shell}) and the fractional contribution to light absorption (f_{BC}, f_{Lens}, f_{Shell}) are shown in Fig. 9. Broadly similar patterns were observed for D_{Shell}, k_{Shell}, and f_{Shell} with O_x. D_{Shell} and E_{abs} tended to be lower in early morning and evening, which was in accordance with anthropogenic activity (with a high CO concentration, as shown in Fig. 5). Peak values of D_{Shell}, k_{Shell}, and f_{Shell} appeared in the mid-afternoon, which corresponded to a more intense photochemical processing and extensive secondary aerosol generation and resulted in a thicker and more absorbing coating shell. The fractional contribution of f_{BC}, f_{Lens}, and f_{Shell} ranged from 35 % to 49 %, 35 % to 42 %, and 11 % to 30 %, respectively, with a mean value of 43 % ± 4 %, 39 % ± 2 %, and 18 % ± 5 %. A ternary plot is shown in the Supplement Fig. S15. Our results suggest that the contribution of the lensing effect to absorption enhancement is limited (Bond and Bergstrom, 2006). The lensing effect is reduced due to the greater absorption of the shell (Lack and Cappa, 2010). The change in optical properties at higher oxidant conditions implies a non-negligible contribution of absorbing secondary aerosol material to photochemistry and should receive more attention in climate modelling (Jo et al., 2016).

4 Conclusions

In this work, the size-resolved mixing state of atmospheric BC particles, light absorption enhancement, and SSA at $\lambda = 532$ nm was measured at a rural site in east China in the summer of 2016. The volatility measurement shows that atmospheric BC particles were well-aged. A single-particle core–shell Mie theory that connected E_{abs} and SSA was developed to interpret the observation. Although further improvements of the calculation with size-distributed BC core and coated shell may give a more complete model, the model used currently with a fixed BC core diameter was found to be useful in illustrating the aging process. In our summertime observations, the increase in f_{Shell} suggests that photochemistry plays a role in modifying BC absorption and indicates that light-absorbing organic compounds require more attention in climate modelling.

Data availability. The data used in this study are available upon request; please contact Weixiong Zhao (wxzhao@aiofm.ac.cn) or Xuezhe Xu (xzxu@aiofm.ac.cn).

Supplement. The supplement related to this article is available online at: https://doi.org/10.5194/acp-18-16829-2018-supplement.

Author contributions. XX, WZ, and WZ designed the research and organized the field measurements. XQ conducted VTDMA measurements. XX, SW, QZ, and BF conducted optical measurements. YH, XD, BW, XL, SZ, and YT conducted the measurement of trace pollutants. XX, WZ, XQ, SW, DSV, and WC analysed data. XX, WZ, SW, DSV, and WC wrote the paper. All authors discussed the results and commented on the paper.

Competing interests. The authors declare that they have no conflict of interest.

Acknowledgements. This research was supported by the National Natural Science Foundation of China (41330424), the Natural Science Foundation of Anhui Province (1508085J03), the Youth Innovation Promotion Association CAS (2016383), and the China Special Fund for Meteorological Research in the Public Interest (GYHY201406039).

Edited by: James Allan
Reviewed by: two anonymous referees

References

Bluvshtein, N., Flores, J. M., Segev, L., and Rudich, Y.: A new approach for retrieving the UV-vis optical properties of ambient aerosols, Atmos. Meas. Tech., 9, 3477–3490, https://doi.org/10.5194/amt-9-3477-2016, 2016.

Bohren, C. F. and Huffman, D. R.: Absorption and scattering of light by small particles, 530 pp., Wiley, 1983.

Bond, T. C. and Bergstrom, R. W.: Light Absorption by carbonaceous particles: an investigative review, Aerosol Sci. Technol., 40, 27–67, https://doi.org/10.1080/02786820500421521, 2006.

Bond, T. C., Streets, D. G., Yarber, K. F., Nelson, S. M., Woo, J. H., and Klimont, Z.: A technology-based global inventory of black and organic carbon emissions from combustion, J. Geophys. Res.-Atmos., 109, D14203, https://doi.org/10.1029/2003JD003697, 2004.

Bond, T. C., Bhardwaj, E., Dong, R., Jogani, R., Jung, S., Roden, C., Streets, D. G., and Trautmann, N. M.: Historical emissions of black and organic carbon aerosol from energy-related combustion, 1850–2000, Global Biogeochem Cy., 21, GB2018, https://doi.org/10.1029/2006GB002840, 2007.

Bond, T. C., Doherty, S. J., Fahey, D. W., Forster, P. M., Berntsen, T., DeAngelo, B. J., Flanner, M. G., Ghan, S., Kärcher, B., Koch, D., Kinne, S., Kondo, Y., Quinn, P. K., Sarofim, M. C., Schultz, M. G., Schulz, M., Venkataraman, C., Zhang, H., Zhang, S., Bellouin, N., Guttikunda, S. K., Hopke, P. K., Jacobson, M. Z., Kaiser, J. W., Klimont, Z., Lohmann, U., Schwarz, J. P., Shindell, D., Storelvmo, T., Warren, S. G., and Zender, C. S.: Bounding the role of black carbon in the climate system: A scientific assessment, J. Geophys. Res., 118, 5380–5552, https://doi.org/10.1002/jgrd.50171, 2013.

Boucher, O., Balkanski, Y., Hodnebrog, O., Myhre, C. L., Myhre, G., Quaas, J., Samset, B. H., Schutgens, N., Stier, P., and Wang, R.: Jury is still out on the radiative forcing by black carbon, P. Natl. Acad. Sci. USA, 113, E5092–5093, https://doi.org/10.1073/pnas.1607005113, 2016.

Brooks, B. J., Smith, M. H., Hill, M. K., and O'Dowd, C. D.: Size-differentiated volatility analysis of internally mixed laboratory-generated aerosol, J. Aerosol Sci., 33, 555–579, https://doi.org/10.1016/S0021-8502(01)00192-6, 2002.

Cappa, C. D., Onasch, T. B., Massoli, P., Worsnop, D. R., Bates, T. S., Cross, E. S., Davidovits, P., Hakala, J., Hayden, K. L., Jobson, B. T., Kolesar, K. R., Lack, D. A., Lerner, B. M., Li, S. M., Mellon, D., Nuaaman, I., Olfert, J. S., Petäjä, T., Quinn, P. K., Song, C., Subramanian, R., Williams, E. J., and Zaveri, R. A.: Radiative absorption enhancements due to the mixing state of atmospheric black carbon, Science, 337, 1078–1081, https://doi.org/10.1126/science.1223447, 2012.

Cevik, B. K., Rutter, A. P., Gong, L., Griffin, R. J., Flynn, J. H., Lefer, B. L., and Kim, S.: Airmass aging metrics derived from particle and other measurements near Fort Worth, Atmos. Environ, 126, 45–54, https://doi.org/10.1016/j.atmosenv.2015.11.044, 2016.

Chakrabarty, R. K., Moosmüller, H., Chen, L.-W. A., Lewis, K., Arnott, W. P., Mazzoleni, C., Dubey, M. K., Wold, C. E., Hao, W. M., and Kreidenweis, S. M.: Brown carbon in tar balls from smoldering biomass combustion, Atmos. Chem. Phys., 10, 6363–6370, https://doi.org/10.5194/acp-10-6363-2010, 2010.

Chen, B., Bai, Z., Cui, X., Chen, J., Andersson, A., and Gustafsson, O.: Light absorption enhancement of black carbon from urban haze in Northern China winter, Environ. Pollut., 221, 418–426, https://doi.org/10.1016/j.envpol.2016.12.004, 2017.

Cheng, Y., He, K. B., Engling, G., Weber. R., Liu, J. M., Du, Z. Y., and Dong, S. P.: Brown and black carbon in Beijing aerosol: Implications for the effects of brown coating on light absorption by black carbon, Sci. Total Environ., 599–600, 1047–1055, https://doi.org/10.1016/j.scitotenv.2017.05.061, 2017.

Cheng, Y. F., Eichler, H., Wiedensohler, A., Heintzenberg, J., Zhang, Y. H., Hu, M., Herrmann, H., Zeng, L. M., Liu, S., Gnauk, T., Bruggemann, E., and He, L. Y.: Mixing state of elemental carbon and non-light-absorbing aerosol components derived from in situ particle optical properties at Xinken in Pearl River Delta of China, J. Geophys. Res., 111, D20204, https://doi.org/10.1029/2005JD006929, 2006.

Cheng, Y. F., Berghof, M., Garland, R. M., Wiedensohler, A., Wehner, B., Müller, T., Su, H., Zhang, Y. H., Achtert, P., Nowak, A., Pöschl, U., Zhu, T., Hu, M., and Zeng, L. M.: Influence of soot mixing state on aerosol light absorption and single scattering albedo during air mass aging at a polluted regional site in northeastern China, J. Geophys. Res.-Atmos., 114, D00G10, https://doi.org/10.1029/2008jd010883, 2009.

Cheng, Y. F., Su, H., Rose, D., Gunthe, S. S., Berghof, M., Wehner, B., Achtert, P., Nowak, A., Takegawa, N., Kondo, Y., Shiraiwa, M., Gong, Y. G., Shao, M., Hu, M., Zhu, T., Zhang, Y. H., Carmichael, G. R., Wiedensohler, A., Andreae, M. O., and Pöschl, U.: Size-resolved measurement of the mixing state of soot in the megacity Beijing, China: diurnal cycle, aging and parameterization, Atmos. Chem. Phys., 12, 4477–4491, https://doi.org/10.5194/acp-12-4477-2012, 2012.

Cheung, H. H. Y., Tan, H., Xu, H., Li, F., Wu, C., Yu, J. Z., and Chan, C. K.: Measurements of non-volatile aerosols with a VTDMA and their correlations with carbonaceous aerosols in Guangzhou, China, Atmos. Chem. Phys., 16, 8431–8446, https://doi.org/10.5194/acp-16-8431-2016, 2016.

China, S., Scarnato, B., Owen, R. C., Zhang, B., Ampadu, M. T., Kumar, S., Dzepina, K., Dziobak, M. P., Fialho, P., Perlinger, J. A., Hueber, J., Helmig, D., Mazzoleni, L. R., and Mazzoleni, C.: Morphology and mixing state of aged soot particles at a remote marine free troposphere site: Implications for optical properties, Geophys. Res. Lett., 42, 1243–1250, https://doi.org/10.1002/2014GL062404, 2015.

Cui, F., Chen, M., Ma, Y., Zheng, J., Zhou, Y., Li, S., Qi, L., and Wang, L.: An intensive study on aerosol optical properties and affecting factors in Nanjing, China, J. Environ. Sci., 40, 35–43, https://doi.org/10.1016/j.jes.2015.08.017, 2016.

Cui, X., Wang, X., Yang, L., Chen, B., Chen, J., Andersson, A., and Gustafsson, Ö.: Radiative absorption enhancement from coatings on black carbon aerosols, Sci. Total Environ., 551, 51–56, https://doi.org/10.1016/j.scitotenv.2016.02.026, 2016.

Deng, X., Shi, C., Wu, B., Chen, Z., Nie, S., He, D., and Zhang, H.: Analysis of aerosol characteristics and their relationships with meteorological parameters over Anhui province in China, Atmos. Res., 109–110, 52–63, https://doi.org/10.1016/j.atmosres.2012.02.011, 2012.

Deolal, S. P., Brunner, D., Steinbacher, M., Weers, U., and Staehelin, J.: Long-term in situ measurements of NO_x and NO_y at Jungfraujoch 1998–2009: time series analysis and evaluation, Atmos. Chem. Phys., 12, 2551–2566, https://doi.org/10.5194/acp-12-2551-2012, 2012.

Dial, K. D., Hiemstra, S., and Thompson, J. E.: Simultaneous measurement of optical scattering and extinction on dispersed aerosol samples, Anal. Chem., 82, 7885–7896, https://doi.org/10.1021/ac100617j, 2010.

Ervens, B., Cubison, M. J., Andrews, E., Feingold, G., Ogren, J. A., Jimenez, J. L., Quinn, P. K., Bates, T. S., Wang, J., Zhang, Q., Coe, H., Flynn, M., and Allan, J. D.: CCN predictions using simplified assumptions of organic aerosol composition and mixing state: a synthesis from six different locations, Atmos. Chem. Phys., 10, 4795–4807, https://doi.org/10.5194/acp-10-4795-2010, 2010.

Fan, X., Chen, H., Xia, X., Li, Z., and Cribb, M.: Aerosol optical properties from the Atmospheric Radiation Measurement Mo-

bile Facility at Shouxian, China, J. Geophys. Res., 115, D00K33, https://doi.org/10.1029/2010JD014650, 2010.

Fang, B., Zhao, W., Xu, X., Zhou, J., Ma, X., Wang, S., Zhang, W., Venables, D. S., and Chen, W.: Portable broadband cavity-enhanced spectrometer utilizing Kalman filtering: application to real-time, in situ monitoring of glyoxal and nitrogen dioxide, Opt. Exp., 25, 26910–26922, https://doi.org/10.1364/OE.25.026910, 2017.

Fierz, M., Vernooij, M. G., and Burtscher, H.: An improved low-flow thermodenuder, J. Aerosol Sci., 38, 1163–1168, https://doi.org/10.1016/j.jaerosci.2007.08.006, 2007.

Forestieri, S. D., Helgestad, T. M., Lambe, A. T., Renbaum-Wolff, L., Lack, D. A., Massoli, P., Cross, E. S., Dubey, M. K., Mazzoleni, C., Olfert, J. S., Sedlacek III, A. J., Freedman, A., Davidovits, P., Onasch, T. B., and Cappa, C. D.: Measurement and modeling of the multiwavelength optical properties of uncoated flame-generated soot, Atmos. Chem. Phys., 18, 12141–12159, https://doi.org/10.5194/acp-18-12141-2018, 2018.

Gustafsson, O. and Ramanathan, V.: Convergence on climate warming by black carbon aerosols, P. Natl. Acad. Sci. USA, 113, 4243–4245, https://doi.org/10.1073/pnas.1603570113, 2016.

Hallquist, M., Munthe, J., Hu, M., Wang, T., Chan, C. K., Gao, J., Boman, J., Guo, S., Hallquist, Å. M., Mellqvist, J., Moldanova, J., Pathak, R. K., Pettersson, J. B. C., Pleijel, H., Simpson, D., and Thynell, M.: Photochemical smog in China: scientific challenges and implications for air-quality policies, Natl. Sci. Rev., 3, 401–403, https://doi.org/10.1093/nsr/nww080, 2016.

Han, T., Xu, W., Li, J., Freedman, A., Zhao, J., Wang, Q., Chen, C., Zhang, Y., Wang, Z., Fu, P., Liu, X., and Sun, Y.: Aerosol optical properties measurements by a CAPS single scattering albedo monitor: Comparisons between summer and winter in Beijing, China, J. Geophys. Res., 122, 2513–2526, https://doi.org/10.1002/2016jd025762, 2017.

He, C., Liou, K.-N., Takano, Y., Zhang, R., Levy Zamora, M., Yang, P., Li, Q., and Leung, L. R.: Variation of the radiative properties during black carbon aging: theoretical and experimental intercomparison, Atmos. Chem. Phys., 15, 11967–11980, https://doi.org/10.5194/acp-15-11967-2015, 2015.

He, C., Takano, Y., Liou, K.-N., Yang, P., Li, Q., and Mackowski, D. W.: Intercomparison of the GOS approach, superposition T matrix method, and laboratory measurements for black carbon optical properties during aging, J. Quant. Spectrosc. Radiat. Transf., 184, 287–296, https://doi.org/10.1016/j.jqsrt.2016.08.004, 2016.

Jacobson, M. Z.: Strong radiative heating due to the mixing state of black carbon in atmospheric aerosols, Nature, 409, 695–697, https://doi.org/10.1038/35055518, 2001.

Ji, D. S., Gao, W. K, Zhang, J. K, Yu, M., Zhou, L. X., Yu, P. F., Li, Y., Sun, J. R., Ge, B. Z., Tang, G. Q., Sun, Y. L., and Wang, Y. S.: Investigating the evolution of summertime secondary atmospheric pollutants in urban Beijing, Sci. Total Environ., 572, 289–300, https://doi.org/10.1016/j.scitotenv.2016.07.153, 2016.

Jo, D. S., Park, R. J., Lee, S., Kim, S.-W., and Zhang, X.: A global simulation of brown carbon: implications for photochemistry and direct radiative effect, Atmos. Chem. Phys., 16, 3413–3432, https://doi.org/10.5194/acp-16-3413-2016, 2016.

Jo, D. S., Park, R. J., Jeong, J. I., Curci, G., Lee, H.-M., and Kim, S.-W.: Key factors affecting single scattering albedo calculation: Implications for aerosol climate forcing, Atmos. Chem. Phys. Discuss., https://doi.org/10.5194/acp-2017-1104, 2017.

Knox, A., Evans, G. J., Brook, J. R., Yao, X., Jeong, C. H., Godri, K. J., Sabaliauskas, K., and Slowik, J. G.: Mass absorption cross section of ambient black carbon aerosol in relation to chemical age, Aerosol Sci. Tech., 43, 522–532, https://doi.org/10.1080/02786820902777207, 2009.

Krasowsky, T. S., McMeeking, G. R., Wang, D., Sioutas, C., and Ban-Weiss, G. A.: Measurements of the impact of atmospheric aging on physical and optical properties of ambient black carbon particles in Los Angeles, Atmos. Environ., 142, 496–504, https://doi.org/10.1016/j.atmosenv.2016.08.010, 2016.

Lack, D. A. and Cappa, C. D.: Impact of brown and clear carbon on light absorption enhancement, single scatter albedo and absorption wavelength dependence of black carbon, Atmos. Chem. Phys., 10, 4207–4220, https://doi.org/10.5194/acp-10-4207-2010, 2010.

Lack, D. A., Langridge, J. M., Bahreini, R., Cappa, C. D., Middlebrook, A. M., and Schwarz, J. P.: Brown carbon and internal mixing in biomass burning particles, P. Natl. Acad. Sci. USA, 109, 14802–14807, https://doi.org/10.1073/pnas.1206575109, 2012.

Lan, Z. J., Huang, X. F., Yu, K. Y., Sun, T. L., Zeng, L. W., and Hu, M.: Light absorption of black carbon aerosol and its enhancement by mixing state in an urban atmosphere in South China, Atmos. Environ., 69, 118–123, https://doi.org/10.1016/j.atmosenv.2012.12.009, 2013.

Li, Z., Li, C., Chen, H., Tsay, S.-C., Holben, B., Huang, J., Li, B., Maring, H., Qian, Y., Shi, G., Xia, X., Yin, Y., Zheng, Y., and Zhuang, G.: East Asian studies of tropospheric aerosols and their impact on regional Climate (EAST-AIRC): an overview, J. Geophys. Res., 116, D00K34, https://doi.org/10.1029/2010jd015257, 2011.

Liu, D., Whitehead, J., Alfarra, M. R., Reyes-Villegas, E., Spracklen, D. V., Reddington, C. L., Kong, S., Williams, P. I., Ting, Y.-C., Haslett, S., Taylor, J. W., Flynn, M. J., Morgan, W. T., McFiggans, G., Coe, H., and Allan, J. D.: Black-carbon absorption enhancement in the atmosphere determined by particle mixing state, Nature Geosci., 10, 184–188, https://doi.org/10.1038/ngeo2901, 2017.

Liu, P. F., Zhang, Y., and Martin, S. T.: Complex refractive indices of thin films of secondary organic materials by spectroscopic ellipsometry from 220 to 1200 nm, Environ. Sci. Technol., 47, 13594–13601, https://doi.org/10.1021/es403411e, 2013.

Liu, P. F., Abdelmalki, N., Hung, H.-M., Wang, Y., Brune, W. H., and Martin, S. T.: Ultraviolet and visible complex refractive indices of secondary organic material produced by photooxidation of the aromatic compounds toluene and m-xylene, Atmos. Chem. Phys., 15, 1435–1446, https://doi.org/10.5194/acp-15-1435-2015, 2015.

Liu, S., Aiken, A. C., Gorkowski, K., Dubey, M. K., Cappa, C. D., Williams, L. R., Herndon, S. C., Massoli, P., Fortner, E. C., Chhabra, P. S., Brooks, W. A., Onasch, T. B., Jayne, J. T., Worsnop, D. R., China, S., Sharma, N., Mazzoleni, C., Xu, L., Ng, N. L., Liu, D., Allan, J. D., Lee, J. D., Fleming, Z. L., Mohr, C., Zotter, P., Szidat, S., and Prevot, A. S. H.: Enhanced light absorption by mixed source black and brown carbon particles in UK winter, Nat. Commun., 6, 8435, https://doi.org/10.1038/ncomms9435, 2015.

Ma, N., Zhao, C. S., Müller, T., Cheng, Y. F., Liu, P. F., Deng, Z. Z., Xu, W. Y., Ran, L., Nekat, B., van Pinxteren, D., Gnauk, T., Müller, K., Herrmann, H., Yan, P., Zhou, X. J., and Wiedensohler,

A.: A new method to determine the mixing state of light absorbing carbonaceous using the measured aerosol optical properties and number size distributions, Atmos. Chem. Phys., 12, 2381–2397, https://doi.org/10.5194/acp-12-2381-2012, 2012.

Moffet, R. C. and Prather, K. A.: In-situ measurements of the mixing state and optical properties of soot with implications for radiative forcing estimates, P. Natl. Acad. Sci. USA, 106, 11872–11877, https://doi.org/10.1073/pnas.0900040106, 2009.

Nakayama, T., Ikeda, Y., Sawada, Y., Setoguchi, Y., Ogawa, S., Kawana, K., Mochida, M., Ikemori, F., Matsumoto, K., and Matsumi, Y.: Properties of light-absorbing aerosols in the Nagoya urban area, Japan, in August 2011 and January 2012: Contributions of brown carbon and lensing effect, J. Geophys. Res.-Atmos., 119, 12721–12739, https://doi.org/10.1002/2014JD021744, 2014.

Novakov, T., Ramanathan, V., Hansen, J. E., Kirchstetter, T. W., Sato, M., Sinton, J. E., and Sathaye, J. A.: Large historical changes of fossil-fuel black carbon aerosols, Geophys. Res. Lett., 30, 1324, https://doi.org/10.1029/2002gl016345, 2003.

Olson, M. R., Garcia, M. V., Robinson, M. A., Van Rooy, P., Dietenberger, M. A., Bergin, M., and Schauer, J. J.: Investigation of black and brown carbon multiple-wavelength-dependent light absorption from biomass and fossil fuel combustion source emissions, J. Geophys. Res.-Atmos., 120, 6682–6697, https://doi.org/10.1002/2014JD022970, 2015.

Onasch, T. B., Massoli, P., Kebabian, P. L., Hills, F. B., Bacon, F. W., and Freedman, A.: Single scattering albedo monitor for airborne particulates, Aerosol. Sci. Technol., 49, 267–279, https://doi.org/10.1080/02786826.2015.1022248, 2015.

Paciga, A., Karnezi, E., Kostenidou, E., Hildebrandt, L., Psichoudaki, M., Engelhart, G. J., Lee, B.-H., Crippa, M., Prévôt, A. S. H., Baltensperger, U., and Pandis, S. N.: Volatility of organic aerosol and its components in the megacity of Paris, Atmos. Chem. Phys., 16, 2013–2023, https://doi.org/10.5194/acp-16-2013-2016, 2016.

Peng, J., Hu, M., Guo, S., Du, Z., Zheng, J., Shang, D., Zamora, M. L., Zeng, L., Shao, M., Wu, Y. S., Zheng, J., Wang, Y., Glen, C. R., Collins, D. R., Molina, M. J., and Zhang, R.: Markedly enhanced absorption and direct radiative forcing of black carbon under polluted urban environments, P. Natl. Acad. Sci. USA, 113, 4266–4271, https://doi.org/10.1073/pnas.1602310113, 2016.

Petzold, A., Ogren, J. A., Fiebig, M., Laj, P., Li, S.-M., Baltensperger, U., Holzer-Popp, T., Kinne, S., Pappalardo, G., Sugimoto, N., Wehrli, C., Wiedensohler, A., and Zhang, X.-Y.: Recommendations for reporting "black carbon" measurements, Atmos. Chem. Phys., 13, 8365–8379, https://doi.org/10.5194/acp-13-8365-2013, 2013.

Philippin, S., Wiedensohler, A., and Stratmann, F.: Measurements of non-volatile fractions of pollution aerosols with an eight-tube volatility tandem differential mobility analyzer (VTDMA-8), J. Aerosol Sci., 35, 185–203, https://doi.org/10.1016/j.jaerosci.2003.07.004, 2004.

Ramanathan, V. and Carmichael, G.: Global and regional climate changes due to black carbon, Nature Geosci., 1, 221–227, https://doi.org/10.1038/ngeo156, 2008.

Radney, J. G., You, R., Ma, X., Conny, J. M., Zachariah, M. R., Hodges, J. T., and Zangmeister, C. D.: Dependence of soot optical properties on particle morphology: measurements and model comparisons, Environ. Sci. Technol., 48, 3169–3176, https://doi.org/10.1021/es4041804, 2014.

Saleh, R., Marks, M., Heo, J., Adams, P. J., Donahue, N. M., and Robinson, A. L.: Contribution of brown carbon and lensing to the direct radiative effect of carbonaceous aerosols from biomass and biofuel burning emissions, J. Geophys. Res.-Atmos. 120, 10285–10296, https://doi.org/10.1002/2015JD023697, 2015.

Scarnato, B. V., Vahidinia, S., Richard, D. T., and Kirchstetter, T. W.: Effects of internal mixing and aggregate morphology on optical properties of black carbon using a discrete dipole approximation model, Atmos. Chem. Phys., 13, 5089–5101, https://doi.org/10.5194/acp-13-5089-2013, 2013.

Schwarz, J. P., Spackman, J. R., Fahey, D.W., Gao, R. S., Lohmann, U., Stier, P., Watts, L. A., Thomson, D. S., Lack, D. A., Pfister, L., Mahoney, M. J., Baumgardner, D.,Wilson, J. C., and Reeves, J. M.: Coatings and their enhancement of black carbon light absorption in the tropical atmosphere, J. Geophys. Res.-Atmos., 113, D03203, https://doi.org/10.1029/2007jd009042, 2008.

Slowik, J. G., Stainken, K., Davidovits, P., Williams, L. R., Jayne, J. T., Kolb, C. E., Worsnop, D. R., Rudich, Y., DeCarlo, P. F., and Jimenez, J. L.: Particle morphology and density characterization by combined mobility and aerodynamic diameter measurements. Part 2: application to combustion-generated soot aerosols as a function of fuel equivalence ratio, Aerosol Sci. Technol., 38, 1206–1222, https://doi.org/10.1080/027868290903916, 2004.

Thamban, N. M., Tripathi, S. N., Moosakutty, S. P., Kuntamukkala, P., and Kanawade, V. P.: Internally mixed black cabon in the Indo-Gangetic Plain and its effect on absorption enhancement, Atmos. Res., 197, 211–223, https://doi.org/10.1016/j.atmosres.2017.07.007, 2017.

Ueda, S., Nakayama, T., Taketani, F., Adachi, K., Matsuki, A., Iwamoto, Y., Sadanaga, Y., and Matsumi, Y.: Light absorption and morphological properties of soot-containing aerosols observed at an East Asian outflow site, Noto Peninsula, Japan, Atmos. Chem. Phys., 16, 2525–2541, https://doi.org/10.5194/acp-16-2525-2016, 2016.

Villani, P., Picard, D., Marchand, N., and Laj, P.: Design and validation of a 6-volatility tandem differential mobility analyzer (VTDMA), Aerosol Sci. Technol., 41, 898–906, https://doi.org/10.1080/02786820701534593, 2007.

Wang, Q. Y., Huang, R. J., Cao, J. J., Han, Y. M., Wang, G. H., Li, G. H., Wang, Y. C., Dai, W. T., Zhang, R. J., and Zhou, Y. Q.: Mixing state of black carbon aerosol in a heavily polluted urban area of China: implications for light absorption enhancement, Aerosol. Sci. Technol., 48, 689–697, https://doi.org/10.1080/02786826.2014.917758, 2014.

Wang, Q., Huang, R., Zhao, Z., Cao, J., Ni, H., Tie, X., Zhu, C., Shen, Z., Wang, M., Dai, W., Han, Y., Zhang, N., and Prévôt, A. S. H.: Effects of photochemical oxidation on the mixing state and light absorption of black carbon in the urban atmosphere of China, Environ. Res. Lett., 12, 044012, https://doi.org/10.1088/1748-9326/aa64ea, 2017.

Wang, S., Zhao, W., Xu, X., Fang, B., Zhang, Q., Qian, X., Zhang, W., Chen, W., Pu, W., and Wang, X.: Dependence of columnar aerosol size distribution, optical properties, and chemical components on regional transport in Beijing, Atmos. Environ., 169, 128–139, https://doi.org/10.1016/j.atmosenv.2017.09.016, 2017.

Wang, Y., Liu, F., He, C., Bi, L., Cheng, T., Wang, Z., Zhang, H., Zhang, X., Shi, Z., and Li, W.: Fractal dimen-

sions and mixing structures of soot particles during atmospheric processing, Environ. Sci. Tech. Lett., 4, 487–493, https://doi.org/10.1021/acs.estlett.7b00418, 2017.

Wang, X., Heald, C. L., Ridley, D. A., Schwarz, J. P., Spackman, J. R., Perring, A. E., Coe, H., Liu, D., and Clarke, A. D.: Exploiting simultaneous observational constraints on mass and absorption to estimate the global direct radiative forcing of black carbon and brown carbon, Atmos. Chem. Phys., 14, 10989–11010, https://doi.org/10.5194/acp-14-10989-2014, 2014.

Wehner, B., Berghof, M., Cheng, Y. F., Achtert, P., Birmili, W., Nowak, A., Wiedensohler, A., Garland, R. M., Pöschl, U., Hu, M., and Zhu, T.: Mixing state of nonvolatile aerosol particle fractions and comparison with light absorption in the polluted Beijing region, J. Geophys. Res.-Atmos., 114, D00G17, https://doi.org/10.1029/2008JD010923, 2009.

Wehner B., Philippin, S., and Wiedensohler, A.: Design and calibration of a thermodenuder with an improved heating unit to measure the size-dependent volatile fraction of aerosol particles, J. Aerosol Sci., 33, 1087–1093, https://doi.org/10.1016/S0021-8502(02)00056-3, 2002.

Wu, C., Wu, D., and Yu, J. Z.: Quantifying black carbon light absorption enhancement with a novel statistical approach, Atmos. Chem. Phys., 18, 289–309, https://doi.org/10.5194/acp-18-289-2018, 2018.

Wu, Y., Cheng, T., Liu, D., Allan, J. D., Zheng, L., and Chen, H.: Light absorption enhancement of black carbon constrained by particle morphology, Environ. Sci. Technol, 52, 6912–6919, https://doi.org/10.1021/acs.est.8b00636, 2018.

Xu, X., Zhao, W., Zhang, Q., Wang, S., Fang, B., Chen, W., Venables, D. S., Wang, X., Pu, W., Wang, X., Gao, X., and Zhang, W.: Optical properties of atmospheric fine particles near Beijing during the HOPE-J^{3}A campaign, Atmos. Chem. Phys., 16, 6421–6439, https://doi.org/10.5194/acp-16-6421-2016, 2016.

Zaveri, R. A., Barnard, J. C., Easter, R. C., Riemer, N., and West, M.: Particle-resolved simulation of aerosol size, composition, mixing state, and the associated optical and cloud condensation nuclei activation properties in an evolving urban plume, J. Geophys. Res.-Atmos., 115, D17210, https://doi.org/10.1029/2009JD013616, 2010.

Zhang, R., Khalizov, A. F., Pagels, J., Zhang, D., Xue, H., and McMurry, P. H.: Variability in morphology, hygroscopicity, and optical properties of soot aerosols during atmospheric processing, P. Natl. Acad. Sci. USA, 105, 10291–10296, https://doi.org/10.1073/pnas.0804860105, 2008.

Zhao, W., Xu, X., Dong, M., Chen, W., Gu, X., Hu, C., Huang, Y., Gao, X., Huang, W., and Zhang, W.: Development of a cavity-enhanced aerosol albedometer, Atmos. Meas. Tech., 7, 2551–2566, https://doi.org/10.5194/amt-7-2551-2014, 2014.

Zhou, S., Wang, T., Wang, Z., Li, W., Xu, Z., Wang, X., Yuan, C., Poon, C. N., Louie, P. K. K., Luk, C. W. Y., and Wang, W.: Photochemical evolution of organic aerosols observed in urban plumes from Hong Kong and the Pearl River Delta of China, Atmos. Environ., 88, 219–229, https://doi.org/10.1016/j.atmosenv.2014.01.032, 2014.